Optimal Attitude Control for Spacecraft Using Two Variable-Speed Control Moment Gyros

By Daiki HIGASHIYAMA,[1)] Katsuhiko YAMADA,[1)] and Yasuhiro SHOJI[1)]

[1)]*Graduate School of Engineering, Osaka University, Osaka, Japan*

This paper considers a rest-to-rest spacecraft maneuver using two variable-speed control moment gyros. Two methods of maneuvering time minimization subject to physical constraints are used to derive angular momentum and gimbal angles over time. The first is an analytical method using variational calculus: from the analytical solution, the dynamic characteristics of the attitude maneuver are easily understood, but attitude errors are caused due to the approximations used. These attitude errors can be eliminated by using a numerical method. The numerical method uses a combination of a bisection method and Newton ' s method. These attitude errors are eliminated by a Newton ' s method calculation using the analytical solution as initial values, while the maneuvering time is minimized by the bisection method. The analytical and numerical calculations are executed in all the directions of the attitude maneuver, validating the effectiveness of successful completion of the intended maneuver.

Key Words: Spacecraft, Variable-Speed Control Moment Gyro, Trajectory Generation, Optimal Control

Nomenclature

$\boldsymbol{J}$	:	inertia of spacecraft
$\boldsymbol{\omega}$	:	angular velocity
$\boldsymbol{h}_t$	:	total angular momentum of spacecraft
$\boldsymbol{q}$	:	Euler parameters of spacecraft attitude
$\boldsymbol{q}_f$	:	target attitude of spacecraft
$\hat{\boldsymbol{\alpha}}$	:	unit vector of spacecraft's rotational axis
$\boldsymbol{\theta}$	:	rotational angle of spacecraft
$\hat{\boldsymbol{\alpha}}_f$	:	target of $\hat{\boldsymbol{\alpha}}$
$\boldsymbol{\theta}_f$	:	target of θ
ϕ_i	:	gimbal angle of VSCMG i
h	:	initial angular momentum of VSCMG
h_{wi}	:	angular momentum of VSCMG i
Δh_{wi}	:	variation of h_{wi} from initial value
t_f	:	maneuvering time

Subscript

i	:	number of VSCMG ($i = 1, 2$)

1. Introduction

A control moment gyro (CMG) is an actuator used for spacecraft attitude control. It exchanges angular momentum with the spacecraft by changing the direction of the angular momentum vector of its gimballed wheel. There are two types of CMGs: one is a single-gimbal control moment gyro (SGCMG) with one degree of freedom; another is a double-gimbal control moment gyro (DGCMG) with two degrees of freedom. CMGs have the advantage of generating an output torque that is larger than the input torque. However, CMGs have gimbal angles where the attitude control torques cannot be exactly generated. These singular states are a critical problem for spacecraft attitude control by CMGs.

In order to avoid the singularity problems of CMGs, a variable-speed control moment gyro (VSCMG) has been studied.[1–5)] The wheel speed of a VSCMG is allowed to vary continuously, whereas the wheel speed of a CMG is kept constant. Thus, a VSCMG has one more a degree of freedom than a CMG and can be considered as a hybrid actuator between a CMG and a reaction wheel (RW). A VSCMG has several advantages over CMGs with the same degrees of freedom such as low cost, low power consumption, low weight, and small size.

Singularity avoidance utilizing the mechanical characteristics of the torque vector generated by a RW, which is always perpendicular to that generated by a CMG, has been studied.[1–5)] In other research, a smaller number of VSCMGs have been made to control the spacecraft attitude than would have been needed if CMGs were used. Taking this process further, the spacecraft attitude can be controlled using one double-gimbal variable-speed control moment gyro (DGVSCMG), which is an actuator with three degrees of freedom. Spacecraft attitude control using a DGVSCMG has also been extensively researched.[6–11)] In the case of a single-gimbal variable-speed control moment gyro (SGVSCMG), spacecraft pointing is achieved using two degrees of freedom.[12,13)]

This paper discusses a rest-to-rest spacecraft maneuver using two SGVSCMGs. Time trajectories of angular momentums and gimbal angles are derived analytically and numerically with the goal of minimizing maneuvering time subject to a set of physical constraints. The analytical and numerical calculations are executed in all the directions of the attitude maneuver. The analytical and numerical solutions are almost the same in maneuvering time and the maneuvering time surface is asymmetric. The characteristics of that asymmetry are also discussed in this paper.

2. Equation of motion

Two SGVSCMGs are arranged as shown in Fig. 1, where each SGVSCMG is identified as either VSCMG1 or VSCMG2. The x, y, and z axes in Fig. 1 constitute coordinates of a spacecraft-fixed frame. The VSCMG1 is arranged such that the gimbal axis and the angular momentum vector in its nominal gimbal angle are aligned with the $+z$-axis and $+x$-axis, respec-

tively, whereas the VSCMG2 is arranged such that the gimbal axis and the angular momentum vector in its nominal gimbal angle are aligned with the $+y$-axis and $-x$-axis, respectively. The total angular momentum of the spacecraft is expressed as

$$\boldsymbol{h}_t = \boldsymbol{J}\boldsymbol{\omega} + h_{w1}\begin{bmatrix}\cos\phi_1\\ \sin\phi_1\\ 0\end{bmatrix} + h_{w2}\begin{bmatrix}-\cos\phi_2\\ 0\\ \sin\phi_2\end{bmatrix}. \tag{1}$$

The angular velocity of the spacecraft is assumed to be zero at the initial state, and the gimbal angles of the VSCMGs are in the nominal position (the gimbal angles are 0 degree) at the initial state. The angular momentum of the VSCMGs cancel each other at the initial state, thus the total angular momentum of the spacecraft is conserved at zero during the attitude maneuver. The equation of motion is expressed as

$$\boldsymbol{J}\dot{\boldsymbol{\omega}} + \boldsymbol{\omega}\times\boldsymbol{h}_t = \boldsymbol{B}\boldsymbol{u}, \tag{2}$$

where $\boldsymbol{B}$ and $\boldsymbol{u}$ are given by

$$\boldsymbol{B} = -\begin{bmatrix}\cos\phi_1 & -\sin\phi_1 & -\cos\phi_2 & \sin\phi_2\\ \sin\phi_1 & \cos\phi_1 & 0 & 0\\ 0 & 0 & \sin\phi_2 & \cos\phi_2\end{bmatrix}, \tag{3}$$

$$\boldsymbol{u} = \begin{bmatrix}\dot{h}_{w1} & h_{w1}\dot{\phi}_1 & \dot{h}_{w2} & h_{w2}\dot{\phi}_2\end{bmatrix}^{\mathrm{T}}. \tag{4}$$

The spacecraft attitude is expressed by the Euler parameters $\boldsymbol{q}$. This is expressed as

$$\boldsymbol{q} = \begin{bmatrix}q_1 & q_2 & q_3 & q_4\end{bmatrix},^{\mathrm{T}} \tag{5}$$

where q_1, q_2, q_3, and q_4 are given by

$$\begin{bmatrix}q_1\\ q_2\\ q_3\end{bmatrix} = \hat{\boldsymbol{\alpha}}\sin\frac{\theta}{2},\ q_4 = \cos\frac{\theta}{2}. \tag{6}$$

The Euler parameters are related to the angular velocity of the spacecraft by the following equation:

$$\dot{\boldsymbol{q}} = \frac{1}{2}\boldsymbol{q}\otimes\boldsymbol{\omega}, \tag{7}$$

where $\otimes$ denotes a quaternion multiplication.

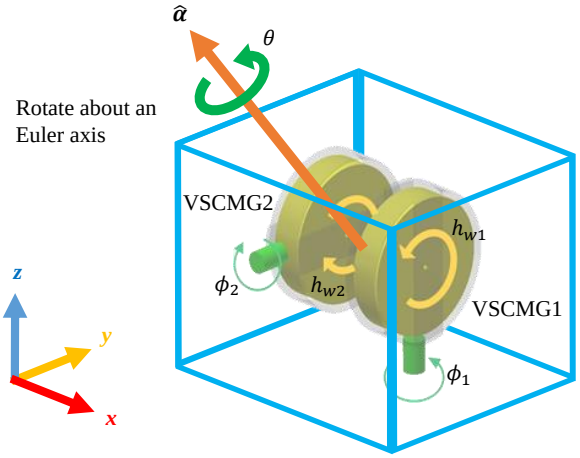

Fig. 1. Arrangement of VSCMGs.

3. Optimal trajectories

3.1. Rest-to-rest maneuvering

In this paper, rest-to-rest attitude maneuvers using two SGVSCMGs are considered. The initial and final angular velocities of the spacecraft are both zero. In order for the CMGs to output sufficiently large torque values, the magnitude of the wheel angular momentums must be maintained within a certain range, as it is proportional to the torque exerted by CMGs. Moreover, there are constraints on both the gimbal rates and the wheel torques because of mechanical limitations.

The target attitude of the spacecraft, $\boldsymbol{q}_f$, is expressed as

$$\boldsymbol{q}_f = \begin{bmatrix}q_{1f} & q_{2f} & q_{3f} & q_{4f}\end{bmatrix},^{\mathrm{T}} \tag{8}$$

where q_{1f}, q_{2f}, q_{3f} and q_{4f} are given by

$$\begin{bmatrix}q_{1f} & q_{2f} & q_{3f}\end{bmatrix}^{\mathrm{T}} = \hat{\boldsymbol{\alpha}}_f\sin\frac{\theta_f}{2},\ q_4 = \cos\frac{\theta_f}{2}. \tag{9}$$

3.2. Approximation of the model

In order to obtain analytically the optimal trajectories of the gimbal angles and the wheel angular momentums, the variations of the Euler parameters $\boldsymbol{q}$, the gimbal angles ϕ_i, and the wheel angular momentums h_{wi} from the nominal values are assumed to be small. Based on these assumptions, the input matrix $\boldsymbol{B}$ is rewritten as

$$\boldsymbol{B} = -\begin{bmatrix}1 & -\phi_1 & -1 & \phi_2\\ \phi_1 & 1 & 0 & 0\\ 0 & 0 & \phi_2 & 1\end{bmatrix}. \tag{10}$$

Eq. (7) is solved for $\boldsymbol{\omega}$ as

$$\boldsymbol{\omega} = 2\dot{\boldsymbol{q}}^{\dagger}\otimes\boldsymbol{q}, \tag{11}$$

and it is simplified to

$$\boldsymbol{\omega} = 2\begin{bmatrix}q_4\dot{q}_1 - q_1\dot{q}_4 - q_2\dot{q}_3 + q_3\dot{q}_2\\ q_4\dot{q}_2 - q_2\dot{q}_4 - q_3\dot{q}_1 + q_1\dot{q}_3\\ q_4\dot{q}_3 - q_3\dot{q}_4 - q_1\dot{q}_2 + q_1\dot{q}_2\end{bmatrix}. \tag{12}$$

The angular velocity $\boldsymbol{\omega}$ is approximated to

$$\boldsymbol{\omega} = 2\begin{bmatrix}\dot{q}_1\\ \dot{q}_2\\ \dot{q}_3\end{bmatrix}. \tag{13}$$

By substituting Eq. (13) into Eq. (2), the following equations are obtained:

$$2J_1\ddot{q}_1 = -\dot{h}_{w1} + \dot{h}_{w2} + h_{w1}\phi_1\dot{\phi}_1 - h_{w2}\phi_2\dot{\phi}_2, \tag{14}$$

$$2J_2\ddot{q}_2 = -\dot{h}_{w1}\phi_1 - h_{w1}\dot{\phi}_1, \tag{15}$$

$$2J_3\ddot{q}_3 = -\dot{h}_{w2}\phi_2 - h_{w2}\dot{\phi}_2. \tag{16}$$

Here, the inertia tensor of the spacecraft is assumed to be diagonal

$$\boldsymbol{J} = \mathrm{diag}\,(J_1,\ J_2,\ J_3). \tag{17}$$

By integrating both sides of Eqs. (14), (15), and (16), they are rewritten as

$$\dot{q}_1 = -\frac{1}{2J_1}\left(\Delta h_{w1} - \Delta h_{w2}\right) + \frac{h}{4J_1}\left({\phi_1}^2 - {\phi_2}^2\right), \tag{18}$$

$$\dot{q}_2 = -\frac{h}{2J_2}\phi_1, \tag{19}$$

$$\dot{q}_3 = -\frac{h}{2J_3}\phi_2, \tag{20}$$

where

$$\Delta h_{w1} = h_{w1} - h,\ \Delta h_{w2} = h_{w2} - h. \tag{21}$$

3.3. Analytical method for resolution of optimal trajectories

This subsection proposes an analytical method by using variational calculus. In this approach, in order to minimize the total energy for the attitude maneuver, $\ddot{\phi}_i$ and $\Delta\ddot{h}_{wi}$ are minimized because $h_{wi}\ddot{\phi}_i$ and $\Delta\ddot{h}_{wi}$ mean the energy per unit time. This variational calculus is divided into two steps by separating Eq. (18) and Eqs. (19) and (20) because it is difficult to simultaneously determine ϕ_i and Δh_{wi}.

First, $\ddot{\phi}_i$ are minimized by using Eqs. (19) and (20). The gimbal angles ϕ_i are determined by minimizing the cost function L_1 given by

$$L_1 = \int_0^{t_f}\left({\ddot{\phi}_1}^2 + {\ddot{\phi}_2}^2\right)dt. \tag{22}$$

Boundary conditions are set as

$$q_2(0) = 0,\ q_3(0) = 0,$$

$$\phi_1(0) = 0,\ \phi_2(0) = 0,\ \dot{\phi}_1(0) = 0,\ \dot{\phi}_2(0) = 0,$$

$$q_2(t_f) = q_{2f},\ q_3(t_f) = q_{3f},$$

$$\phi_1(t_f) = 0,\ \phi_2(t_f) = 0,\ \dot{\phi}_1(t_f) = 0,\ \dot{\phi}_2(t_f) = 0. \tag{23}$$

From this step, time trajectories of the gimbal angles are expressed by polynomial functions as follows:

$$\phi_1 = -\frac{60J_2q_{2f}}{ht_f^5}\left(t^4 - 2t_ft^3 + {t_f}^2t^2\right), \tag{24}$$

$$\phi_2 = -\frac{60J_3q_{3f}}{ht_f^5}\left(t^4 - 2t_ft^3 + {t_f}^2t^2\right). \tag{25}$$

Second, the terms $\Delta\ddot{h}_{wi}$ are minimized by using Eq. (18). Equation (18) is a linear differential equation of q_1, therefore q_1 is represented by the sum of the responses by the first and second terms on the right-hand side. The response by the first term depends on the values of Δh_{w1} and Δh_{w2} and is denoted as $\hat{q}_1$. The response by the second term depends on the values of ϕ_1 and ϕ_2, which are determined in the first step. The component q_1 is rewritten as follows using $\hat{q}_1$:

$$q_1 = \hat{q}_1 + \frac{h}{4J_1}\int_0^{t_f}\left({\phi_1}^2 - {\phi_2}^2\right)dt. \tag{26}$$

The component $\hat{q}_1$ only depends on the values of Δh_{w1} and Δh_{w2} from Eq. (18) as

$$\dot{\hat{q}}_1 = -\frac{1}{2J_1}\left(\Delta h_{w1} - \Delta h_{w2}\right). \tag{27}$$

The terms Δh_{wi} are determined by minimizing the cost function L_2 given by

$$L_2 = \int_0^{t_f}\left({\Delta\ddot{h}_{w1}}^2 + {\Delta\ddot{h}_{w2}}^2\right)dt. \tag{28}$$

In the variational calculus analysis, boundary conditions are set as

$$\hat{q}_1(0) = 0,$$

$$\Delta h_{w1}(0) = 0,\ \Delta h_{w2}(0) = 0,\ \Delta\dot{h}_{w1}(0) = 0,\ \Delta\dot{h}_{w2}(0) = 0,$$

$$\hat{q}_1(t_f) = q_{1f} - \frac{h}{4J_1}\int_0^{t_f}\left({\phi_1}^2 - {\phi_2}^2\right)dt,$$

$$\Delta h_{w1}(t_f) = 0,\ \Delta h_{w2}(t_f) = 0,\ \Delta\dot{h}_{w1}(t_f) = 0,\ \Delta\dot{h}_{w2}(t_f) = 0. \tag{29}$$

From this step, time trajectories of the wheel angular momentums are expressed by polynomial functions as follows:

$$\Delta h_{w1} = -\frac{30J_1\hat{q}_{1f}}{t_f^5}\left(t^4 - 2t_ft^3 + {t_f}^2t^2\right), \tag{30}$$

$$\Delta h_{w2} = \frac{30J_1\hat{q}_{1f}}{t_f^5}\left(t^4 - 2t_ft^3 + {t_f}^2t^2\right). \tag{31}$$

The analytical solutions are expressed as Eqs. (24), (25), (30), and (31). Next, the spacecraft maneuvering time is minimized in order that the wheel angular momentums Δh_{wi}, wheel torques $\Delta\dot{h}_{wi}$, and the gimbal rates $\dot{\phi}_i$ are within the constraints shown in Table 2. However, there are attitude errors in the analytical solution due to its approximations. The attitude errors are eliminated by the following numerical method.

3.4. Numerical method for resolution of optimal trajectories

This subsection proposes a numerical method using the combination of a bisection method and Newton's method. The analytical solution is used as initial values of the Newton's method approach, where the coefficients of the polynomial functions are selected as adjustable parameters. The attitude errors of the analytical solution are converged to zero by the Newton's method approach and the maneuvering time is minimized by the bisection method. The details of the numerical method are shown in Fig. 2.

4. Numerical examples

4.1. Comparison of trajectories

This subsection illustrates the trajectories of the rest-to-rest maneuvers based on both the analytical and numerical methods proposed in the previous section. Table 1 shows the properties of the spacecraft, VSCMG1, and VSCMG2. Table 2 shows the constraints of the gimbal rates, wheel angular momentums, and wheel torques. As a target attitude, the unit vector along the spacecraft's rotational axis $\hat{\boldsymbol{\alpha}}_f$, and the rotational angle of spacecraft θ_f, is selected as

$$\hat{\boldsymbol{\alpha}}_f = \left[\frac{1}{\sqrt{3}}\quad\frac{1}{\sqrt{3}}\quad\frac{1}{\sqrt{3}}\right]^{\mathrm{T}},\ \theta_f = 10\ [\mathrm{deg}]. \tag{32}$$

Figure 4 shows the calculations resulting from both the analytical and numerical methods. In Fig. 4, the broken lines and the

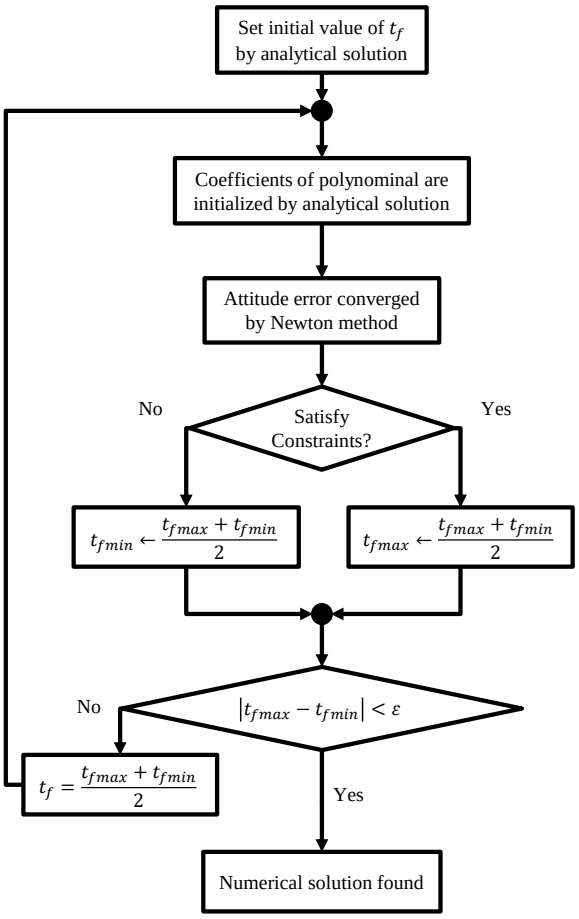

Fig. 2. Flowchart of numerial method.

solid lines show the results of analytical method and those of the numerical one, respectively. Figures 4(a), 4(b), 4(c), 4(d), 4(e), and 4(f) show the attitude, the angular velocity, the gimbal angles, the gimbal rates, the wheel angular momentums, and the wheel torques, respectively. The black horizontal dotted line in Fig. 4(a) denotes the target attitude. The black horizontal lines in Figs. 4(d), 4(e) and 4(f) denote the upper and lower constraints of the variables. The final attitude errors observed in the analytical solution are eliminated in the numerical solution as shown in Fig. 4(a). As shown in Figs. 4(d), 4(e), and 4(f), the constraints of the wheel angular momentums, wheel torques, and gimbal rates are all satisfied.

Table 1. Spacecraft and VSCMGs properties.

inertia of spacecraft	$\boldsymbol{J} = \mathrm{diag}(10, 10, 10)$	kgm^2
initial angular momentum of VSCMG	$h = 1$	Nms

Table 2. Constraints.

wheel angular momentum	$\lvert\Delta h_{wi}\rvert \leq 0.3$	Nms
torpue of wheel	$\lvert\Delta \dot{h}_{wi}\rvert \leq 0.1$	Nm
gimbal rate	$\lvert\dot{\phi}_i\rvert \leq 1.0$	rad/s

4.2. Maneuvering time surfaces

The analytical and numerical calculations are executed in all the directions of the attitude maneuver, and the maneuvering time in each direction is plotted so that the direction from the origin to the plotted point represents that of the rotational axis, and the distance between the origin and the point is proportional to the maneuvering time. Figure 3 shows an example of a maneuvering time surface. Figures 5 and 6 show the maneuvering time surface based on the analytical method and that based on the numerical one, respectively. As shown in these Figures, the analytical solutions and numerical ones are almost the same in the maneuvering time, which shows that the analytical solution from Eqs. (18), (19) and (20) almost expresses the attitude maneuver of the spacecraft using two SGVSCMGs. The maneuvering time is longer in the direction of x-axis than that in the other direction because the torque in this direction is generated by the RW and is relatively smaller than that generated by the CMGs. The maneuvering time surface is asymmetric in both the analytical and numerical methods. Figures 7 and 8 are the x-y section of the maneuvering time surface generated by the numerical solution, and its $x-z$ section, respectively. As shown in Fig. 7, the maneuvering time is longer on the side of $-x$ than that of $+x$, while as shown in Fig. 8, the maneuvering time is longer on the side of $+x$ than that of $-x$. The reason for this asymmetry is explained qualitatively by the dynamic characteristics of the analytical solution. As shown in Eq. (19), the gimbal angle of VSCMG1 has an effect on q_2, and as shown in Eq. (20) the gimbal angle of VSCMG2 has an effect on q_3. Thus, the gimbal of VSCMG1 is driven in the case where the unit vector along the spacecraft ' s rotational axis $\hat{\boldsymbol{\alpha}}_f$ has y-component, whereas the gimbal of VSCMG2 is driven in the case where $\hat{\boldsymbol{\alpha}}_f$ has z-component. Moreover, as shown in Eq. (18), the gimbal angle of VSCMG1 and that of VSCMG2 have effects on $+q_1$ and $-q_1$, respectively. The asymmetry is due to the difference between the effects of the gimbal angle of VSCMG1 and that of VSCMG2 on q_1. For example, consider the case where $\hat{\boldsymbol{\alpha}}_f$ has x and y components. In this case, the gimbal of VSCMG1 is driven for the rotation in the y-direction, while at the same time, q_1 moves in the positive direction due to the influence on $+q_1$. Due to the influence of the VSCMG1 gimbal angle, the maneuvering time is shortened in the case where the target value of q_1 is positive, whereas the maneuvering time is extended in the case where the target value of q_1 is negative. This is the reason for the asymmetry in Fig. 7. Similarly, consider the case where $\hat{\boldsymbol{\alpha}}_f$ has x and z components. In this case, the gimbal of VSCMG2 is driven for the rotation in the z-direction, and at the same time, q_1 moves to a negative direction due to the influence on $-q_1$. Because of the influence of the VSCMG2 gimbal angle, the maneuvering time is shortened in the case where the target value of q_1 is negative, whereas the maneuvering time is extended in the case where the target value of q_1 is positive. This is the reason for the asymmetry in Fig. 8.

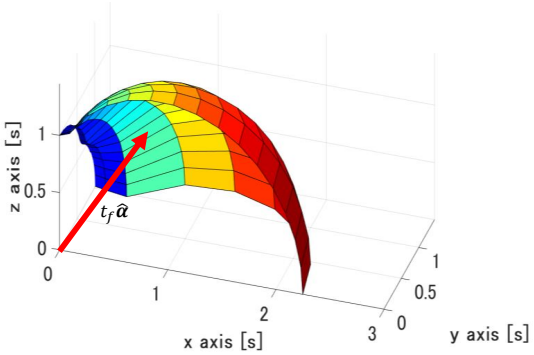

Fig. 3. Example of maneuvering time surface.

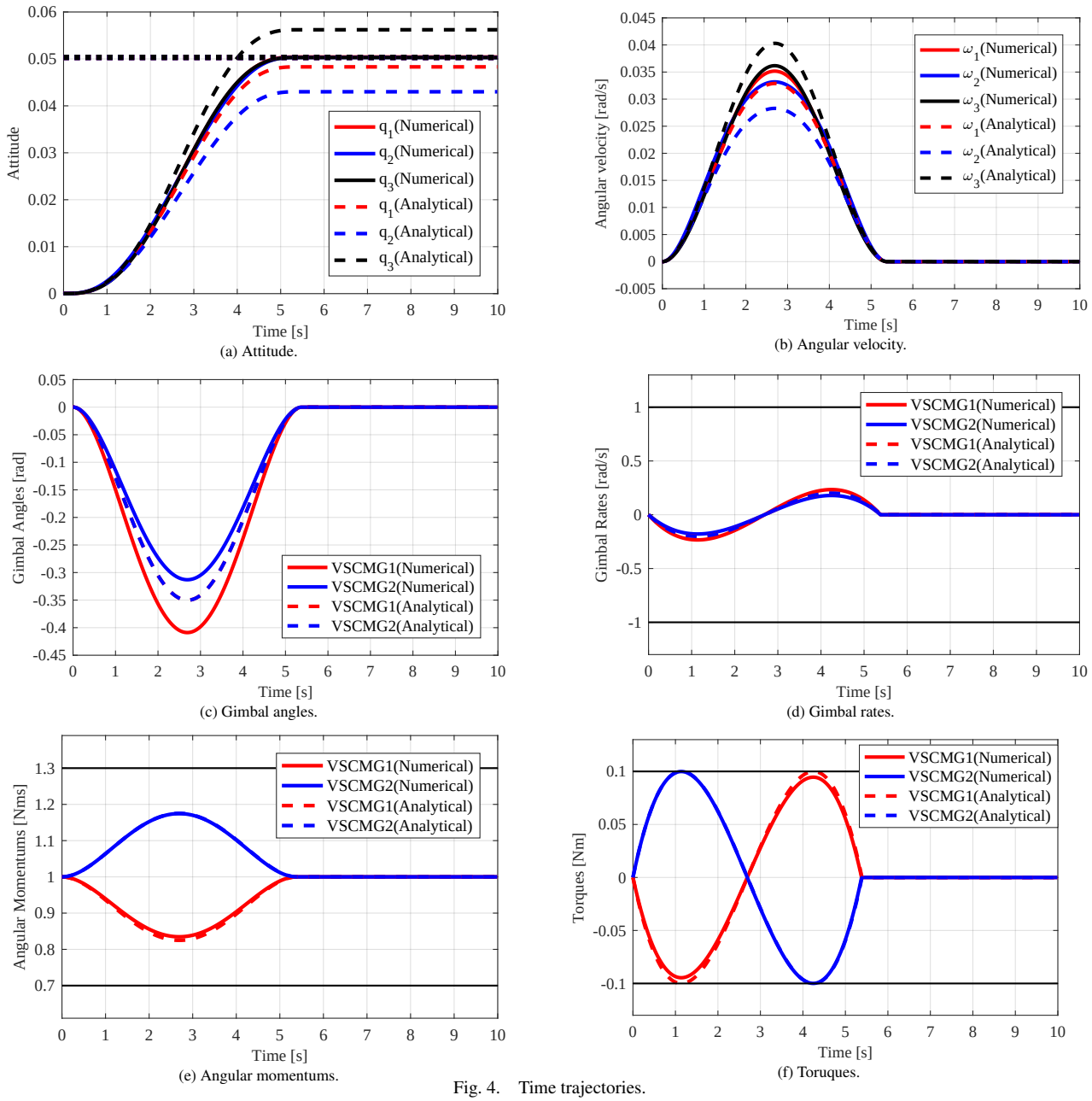

(a) Attitude. (b) Angular velocity. (c) Gimbal angles. (d) Gimbal rates. (e) Angular momentums. (f) Toruques.

Fig. 4. Time trajectories.

5. Conclusion

In this paper, the spacecraft attitude maneuver by using two SGVSCMGs is optimized with the goal of minimizing maneuvering time by both the analytical and numerical methods. The trajectories of the gimbal angles and the wheel angular momentums are derived within the constraints of the gimbal rates, the variation of the wheel angular momentums, and the wheel torques. The analytical and numerical calculations are executed in all the directions of the attitude maneuver, which validates the effectiveness of the trajectory generation technique. Maneuvering times are plotted as a maneuvering time surface, where a point on the surface corresponds to the direction of the rotational axis and the maneuvering time. The asymmetry of the surface is observed in both the analytical and numerical calculations, and a qualitative explanation is given by the dynamic characteristics of the analytical solution. Further studies are needed in order to verify the optimal trajectories experimentally by designing a feedback control law based on the calculated optimal trajectories.

Acknowledgments

This work was supported by JSPS KAKENHI Grant Number JP16K06886.

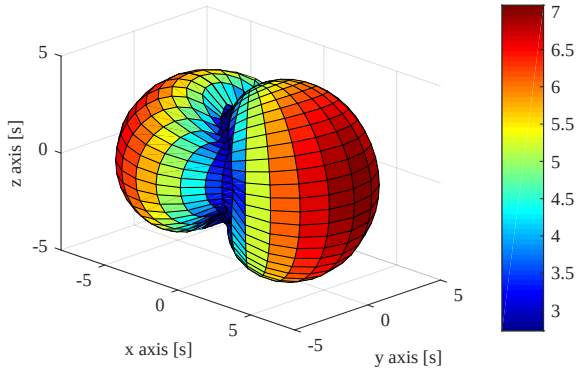

Fig. 5. Maneuvering time surface by analytical solution.

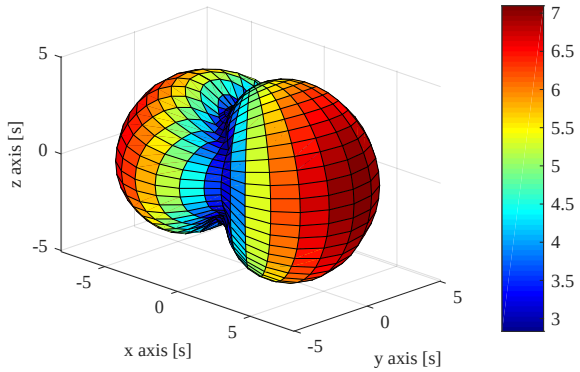

Fig. 6. Maneuvering time surface by numerical solution.

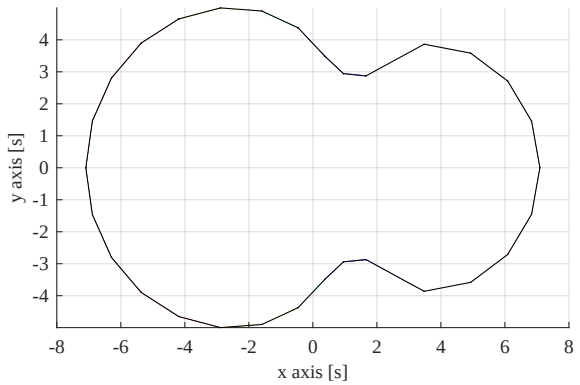

Fig. 7. $x-y$ section of maneuvering time suaface by numerical solution.

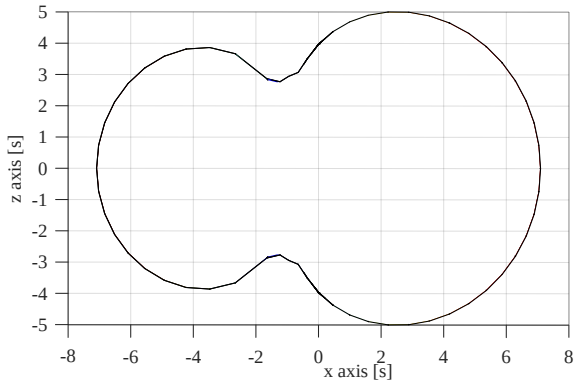

Fig. 8. $x-z$ section of maneuvering time surface by numerical solution.

References

1) Yoon, H. and Tsiotras, P.: Singularity Analysis of Variable-Speed Control Moment Gyros, *Journal of Guidance, Control, and Dynamics*, **27**:**3** (2004), pp.374–386.
2) Romano, M. and Agrawal, B. N.: Attitude Dynamics and Control of a Dual-Body Spacecraft using Variable-Speed Control Moment Gyros, *Journal of Guidance, Control, and Dynamics*, **27**:**4** (2004), pp.513–525.
3) Schaub, H., Vadali, S. R. and Junkins, J. L.: Feedback Control Law for Variable-Speed Control Moment Gyros, *Journal of the Astronautical Sciences*, **46**:**3** (1998), pp. 307–328.
4) McMahon, J. and Schaub, H.: Simplified Singularity Avoidance Using Variable-Speed Control Moment Gyroscope Null Motion, *Journal of Guidance, Control, and Dynamics*, **32**:**6** (2009), pp. 1938–1943.
5) Schaub, H., and Junkins, J. L.: Singularity Avoidance Using Null Motion and Variable-Speed Control Moment Gyros, *Journal of Guidance, Control, and Dynamics*, **23**:**1** (2000), pp. 11–16.
6) Salatun, A. S. and Bainum, P. M.: Analysis of a Double Gimbaled Rection Wheel Spacecraft Attitude Stabilization System, *Acta Astronautica*, **10**:**2** (1983), pp. 55–66.
7) Zhang, H. and Fang, J.: Robust Backstepping Control for Agile Satellite Using Double-Gimbal Variable-Speed Control Moment Gyroscope, *Journal of Guidance, Control, and Dynamics*, **36**:**5** (2013), pp. 105–115.
8) Stevenson, D. and Schaub, H.: Nonlinear Control Analysis of a Double-Gimbal Variable-Speed Control Moment Gyroscope, *Journal of Guidance, Control, and Dynamics*, **35**:**3** (2012), pp. 787–793.
9) Ahmed, J. and Bernstein, D. S.: Adaptive Control of Double-Gimbal Control-Moment Gyro with Unbalanced Rotor, *Journal of Guidance, Control, and Dynamics*, **25**:**1** (2002), pp. 1356–1363.
10) Jikuya, I., Fujii, K. and Yamada, K.: Attitude Maneuver of Spacecraft with a Variable-Speed Control Moment Gyro, *Adv. Space Res*, **58**:**7** (2016), pp. 1303–1317.
11) Tsukahara, T., Yamada, K. and Shoji, Y.: On the Singularity Avoidance/Passage Law of a Variable-speed Double-gimbal Control Moment Gyro, *Aerospace Technology Japan, the Japan Society for Aeronautical and Space Sciences*, **15** (2016), pp. 53–61 (in Japanese).
12) Yamada, K., Takatsuka, N. and Shima, T.: Spacecraft Pointing Control Using aVariable-Speed Control Moment Gyro, *Trans. JSASS Space Tech. Japan*, **7**:**ists26** (2009), pp.Pd_1–Pd_6.
13) Yoon, H. and Tsiotras, P.: Spacecraft Line-of-Sight Control Using a Single Variable-Speed Control Moment Gyro, *Journal of Guidance, Control, and Dynamics*, **29**:**6** (2006), pp.1295–1308.